OPO OPHTHALMIC & PHYSIOLOGICAL OPTICS
THE JOURNAL OF THE COLLEGE OF OPTOMETRISTS

Ophthalmic & Physiological Optics ISSN 0275-5408

Intraocular lens implantation position sensitivity as a function of refractive error

Huanqing Guo, Alexander Goncharov and Chris Dainty

Applied Optics Group, National University of Ireland, Galway, Ireland

Citation information: Guo H, Goncharov A & Dainty C. Intraocular lens implantation position sensitivity as a function of refractive error. *Ophthalmic Physiol Opt* 2011. doi: 10.1111/j.1475-1313.2011.00888.x

Keywords: eye model, intraocular lens, Monte–Carlo simulations, point spread function, refractive error, wavefront aberration

Correspondence: Huanqing Guo
E-mail address: huanqing.guo@nuigalway.ie

Received: 24 January 2011; Accepted: 17 November 2011

Abstract

Purpose: To quantify the change in ocular aberrations due to intraocular lens (IOL) implantation position errors for pseudo-phakic eyes with different refractive errors.

Methods: The theoretical part of this work was based on ray-tracing in emmetropic and myopic eye models. The possible misalignments i.e. the decentration, tilt and axial translation, of the IOLs were statistically combined together and analysed using Monte–Carlo simulations. Spherical IOLs with a 3 and 5 mm pupil and an aspheric IOL with a 5 mm pupil were analysed as a function of refractive error. In the experimental part of the work, we built an IOL optical test bench including a model eye. The white light discrete point spread functions of misaligned IOLs were recorded by a CCD and we compared the change of the spread function as a result of misalignments for two spherical IOLs with different optical powers.

Results: The Monte–Carlo simulations showed that the average root-mean-square spot size at the retinal plane decreased with increasing myopic refractive error, i.e. lower power IOL. The experiments showed that a lower optical power spherical IOL had a less distributed point spread function than a higher optical power IOL, which supported the results of the simulation.

Conclusion: Regarding IOLs designed for myopic patients, low power IOLs (for high myopes) were shown to be less sensitive to the misalignment than high power ones. Aspheric IOLs were more sensitive to position errors than spherical IOLs under the same conditions.

Introduction

An artificial intraocular lens (IOL) is used to replace the cloudy crystalline lens when a person develops cataract. As the population ages, cataract surgery has become the most frequently performed ocular surgical procedure. When the IOL is used to replace the cataractous crystalline lens, one can not only restore vision, but also correct any myopia or hyperopia of the subject.

From the manufacturing point of view, an IOL is a simple lens whose optical properties depend on its material and external shape. Modern IOLs are usually made of polymer plastics such as polymethyl methacrylate (PMMA), acrylic or silicone. The IOL surface design controls the optical power and wavefront aberrations. Both spherical and aspheric surface IOLs have appeared on the market. Aspheric designs attempt to correct as much as possible of the eye's optical defects, such as lower- and higher-order aberrations,[1–4] and polychromatic blur.[5] IOLs cover a wide range of optical powers required for optical correction in cataract patients, who may have refractive errors such as myopia or hyperopia. The prevalence of refractive errors in the elderly population is rather high, especially in some Asian nations.[6–8] The refractive errors have also been linked with biometry of the eye,[9] in particular with the axial length.[10,11] For different levels of refractive errors, IOLs with different powers have different position sensitivity, which will be addressed in this paper.

In order to select IOLs with proper optical powers, appropriate IOL power calculation has become indispensable in cataract surgery. Whereas many empirical IOL power calculation formulas have been developed during the past two decades or so,[12] ray-tracing using eye models also plays an important role in IOL power calculation and optical analysis.[3,13,14] Traditionally these eye models are based on statistical biometric data of the eye. A customized eye model for a specific eye developed from the individual eye's ocular biometry and the wavefront aberrations, has also shown to be a potential tool.[14,15] Ray-tracing in eye models is also useful to analyse IOL implantation position errors (misalignments). The usual way to do this is to introduce different kinds of errors, for example decentrations, tilts and/or defocus into the model and calculate relevant optical quantities such as modulation transfer function (MTF), point spread function (PSF) and image quality. These misalignments can be investigated independently[3,13,14] or in combination.[16–18]

In this research we investigate implantation position errors of IOLs at different levels of refractive error of the eye using ray-tracing eye models, and we also test two IOLs with different optical powers using a physical model eye. To simulate the IOL positions in pseudo-phakic eyes, we combine together the possible position errors of the IOL in the eye models. Monte–Carlo analysis was performed to compute the change of root mean square (RMS) spot size when the IOL was misaligned. We also investigate different contributions of separate types of misalignment. We built a physical model eye that conforms to the international standard for IOL testing. The model eye was used to test the change in the discrete point spread function (DPSF) due to misalignment of IOLs. Here the 'discrete' means the point spread functions were spatially sampled since the DPSF images were recorded by a digital camera. This paper discusses the optical methods and results for quantifying the sensitivity of the IOL to implantation position errors. Eyes with different refractive errors, which need different power IOLs, are investigated as an independent variable. To our knowledge this is the first report that correlates IOL sensitivity to position errors as a function of refractive error.

Methods

The two main methods used in this study were ray-tracing with eye models, and experiments with a physical model eye.

Myopic eye models and Monte–Carlo analysis

Optical models for eyes with refractive errors from 0D to 12D in 2D steps were constructed. We used positive dioptric power to describe the myopic eye refractive error. The biometric data, including the anterior and posterior corneal radius of curvature and asphericity, anterior chamber depth, the lengths of the eye and the chromatic dispersion of different media of the eye, were adopted from Atchison.[9] Atchison[9] reported that higher refractive error myopic eyes have a steeper anterior cornea surface, longer eye length and a more curved retina. The optical surfaces in these models are rotationally symmetric except that the retinal surface is biconic. They were assumed to be aligned on the optical axis and we treated the models as the right eye with the fovea at 4° to the nasal field outside the eye. To replace the crystalline lens, we studied two types of IOLs (n_D = 1.491): spherical ones, and rotationally symmetric aspheric ones. Both types are monofocal and have two equi-convex surfaces. For the aspheric IOL, the aspheric surface is conicoid and faces towards the cornea. The optical design software Zemax (ZEMAX Development Corporation, 2011, http://www.zemax.com) was used to build the models and perform the IOL misalignment analysis.

For both spherical and aspheric IOLs the initial IOL surfaces were optimized in different emmetropic and myopic eye models with a 5 mm pupil size. The IOLs were placed at the estimated equator plane of the crystalline bag that was determined by the cross point obtained by extending the original crystalline lens anterior and posterior rotational symmetric surfaces. Spherical IOLs were also investigated with a 3 mm pupil size. To determine the optimal IOL surfaces, the aberration optimization procedure minimized the optical path difference (OPD) with respect to the mean OPD over the pupil. Five different wavelengths weighted by the photopic spectral sensitivity curve within the visible spectrum (470, 510, 555, 610 and 650 nm) were used in the optimization. Five field points covering 2° of visual field around the fovea were considered; one field point was at the centre and the other four were ±1° around the centre.

The IOL position errors, including decentrations from the optical axis, tilts about the horizontal and vertical axes, and backward and forward axial translations, were investigated. As a polychromatic metric, the RMS spot radius size was used as the retinal plane metric to measure the optical quality due to the misalignments. The change of RMS spot radii was the difference between the RMS spot radius for IOL misalignment position and those for the IOL's initial position. The changes at the five field points and five wavelengths were averaged. Clinically, IOL implantation usually has all the errors combined together rather than only separated single ones. To simulate this, we used the Monte–Carlo method to combine all possibilities. Firstly we defined the permissible ranges of different type of IOL position errors from its

initial position which was set as the origin. Typical errors in pseudo-phakic eyes were considered to determine these ranges.[19–25] Then Gaussian numbers were randomly selected within each of these error ranges, which have a mean zero value. Approximately 70% of the tilted angles were between −3 and +3°, 70% of the decentrations were between −0.3 and +0.3 mm and 70% axial translations were between the range of −0.5 to +0.5 mm. The IOL was then misaligned by amounts determined by these randomly selected numbers. The RMS spot size was subsequently calculated and this was taken as one trial. For example, in one trial the IOL may be simultaneously tilted horizontally by 3.5°, decentred vertically by 0.3 mm and axially translated towards the retina by 0.2 mm. Five hundred and twelve trials were performed and averaged for each refractive error level as one test.

IOL test with the physical model eye

A physical model eye[26] for testing IOLs consists of a simulated 'cornea', IOL and a CCD as the 'retina'. The IOL container was made of BK7 glass in which transparent liquid could be injected. The IOL under test was held in a hollow disc which was placed in the middle of the windows and immersed into the liquid. An achromatic doublet for visible light (Thorlabs, $f = 35.0$ mm, $D = 25.4$ mm; http://www.Thorlabs.com) was placed in front of the window to simulate the cornea. Our aim was to compare the aberration change of the two misaligned IOLs while the contribution of corneal spherical aberration was constant and its effect was negligibe for the 3 mm pupil diameter used in this study. The cornea was taken as aberration free in the experiments so that the IOL was the only source of aberrations. An artificial pupil was placed in front of the cornea and its size made the converging beam have a central circular diameter of 3.0 mm at the IOL location.

Figure 1 shows the optical setup for IOL testing with the physical model eye. A high illuminance white light emitting diode (LED) (Luxeon, 400–750 nm; http://www.philipslumileds.com) was used as the light source with a stabilized power supply (Philips; http://www.Philips.com). A diffuser followed the LED in the optical path to smooth its spatial structure. A 20 micron pinhole was subsequently attached to the diffuser to provide a point source. Neutral density filters were optionally used to modulate the light power in order to not saturate the CCD. A 25 mm diameter, 100 mm focus length achromatic lens (Thorlabs; http://www.Thorlabs.com) was used to collimate the light from the pinhole. The collimated light was then propagated to the physical eye model, passed the 'cornea' and the IOL to the CCD.

The IOL in its container was mounted on horizontal and vertical linear translation stages (Newport; http://www.Newport.com) with 10 micron resolution. The CCD (Retiga 1300, Qimaging; http://www.Qimaging.com) was also mounted on a similar translation stage along the axial direction, which could be moved backward and forward to find the best focus (smallest focal point). The CCD had a pixel size of 6.7 micron square and signal resolution of 12 bits. The advantage of putting the CCD directly following the IOL wet cell was that the DPSF could be recorded and measured in a straightforward manner, and when the IOL was misaligned there would be no optical defects from any additive lenses. The trade-off was that the CCD sample density became critical because of its limited pixel size and discrete sampling which averaged part of the DPSF information. In our experiment the typical DPSF size normally covered from about 9 by 9 to 25 by 25 pixels and the full width at half maximum was from a 3 by 3 to a 8 by 8 pixels round area. We describe three simple metrics for quantifying the DPSF which to some extent eases the restriction of the sampling.

A Matlab (Mathworks, version 2009b; http://www.mathworks.com) computer program was used to calculate the parameters of the DPSF. First the background noise of the images was removed. The centroid coordinates of the DPSFs were calculated by the centre of mass method, which uses the sum of the intensity moments of each pixel divided by the total intensity. Three parameters were

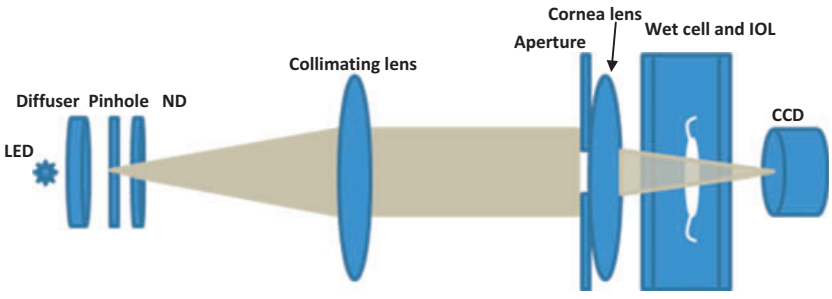

Figure 1. Optical system for testing point spread function of the IOL. The physical model eye consists of the aperture, corneal lens, wet cell with IOL and CCD.

calculated to describe the DPSFs: RMS radius, the trace of inertia matrix and power distribution ratio. The RMS radius was the root-mean-square radial size of the DPSF. The distance between each signal pixel and the centroid was squared and averaged, and then the square root was taken:

$$\text{RMS radius} = \sqrt{\frac{\sum r^2}{N}} \quad (1)$$

where r is the distance from each pixel to the centroid and N is the number of signal pixels. The trace of inertia matrix was calculated by multiplying each pixel with the distance to the centroid squared, summarizing all pixels and then divided by the total intensity:

$$\text{Trace} = \frac{\sum p(r)r^2}{\sum p(r)} \quad (2)$$

where $p(r)$ is the intensity value of each pixel. The RMS radius gave a measure of the geometry spread of all pixels and was measured in microns. The trace of inertia matrix gave a measure of the extent of the area of the DPFS peak and was measured in squared microns. The power distribution ratio was the ratio of the total energy inside the three arc-min area compared to the total energy. The power distribution ratio is a unit-less value and it gave a measure of the degree of light concentration. The above three parameters are independent of the absolute light power.

The IOL DPSF measurement system with the physical model eye was an optical test setup. The aim was to observe the misalignment effect specifically contributed by IOLs. Preliminary experiments were performed to make sure that the model eye itself had no significant effect on the tests. The IOL was removed from the model eye and other parts were kept in place, and then DPSF images were recorded. *Figure 2* shows the results of horizontal decentration of the physical model eye when the IOL is absent. In this figure the RMS radius and the trace of inertia matrix value are kept almost constant with the decentration range used in these experiments. The vertical decentration and axial translation provided similar results which are not shown. Across all the measurements, the average RMS radius, trace of inertia matrix and power ratio were 12.8 ± 0.3 μm, 30.6 ± 1.4 μm^2 and 0.86 ± 0.037, respectively. These results mean that all the DPSF changes measured in the experiments were due to the IOLs.

The IOL was mounted in its disk and placed into its cell with water. At least 30 min was necessary before starting the data collection; this was for the electronics of the CCD and the LED to reach their stable status and the water inside the IOL container to be at the room temperature of about 20°C. The CCD was shifted axially to obtain the smallest PSF for the tested IOL. This CCD location was recorded and taken as the best focus. Neutral density filters were optionally needed to control the flux on the CCD to avoid saturation.

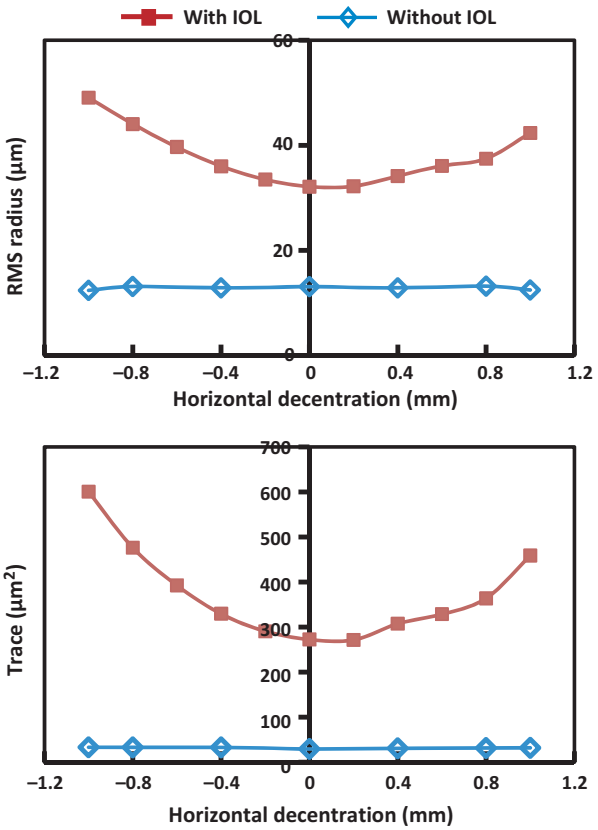

Figure 2. System intrinsic RMS radius and trace of inertia matrix of DPSF measured with the model eye when the IOL was absent. For reference, the horizontal misalignment of the 24.0D IOL has also been shown. When the IOL was absent, the system's RMS and trace response were stable.

The IOL was then manipulated with high precision using the translation stages. The IOL was continuously decentred horizontally or vertically by ±0.2 mm step from the best focus position, and shifted along the optical axis in ±0.1 mm steps. The plus sign represented movements to the right (facing the CCD), upward or towards the cornea.[27] At each altered IOL position, 15 sequential frames of CCD images were acquired and averaged.

Results

Results from ray-tracing eye models

Figure 3 shows the change of RMS spot size (radius) as a function of incremental refractive errors, for the spherical IOLs with 3 and 5 mm pupil size, and the aspheric IOL with 5 mm pupil size. The lines are the linear regressions to the data points. At the same refractive error level, the

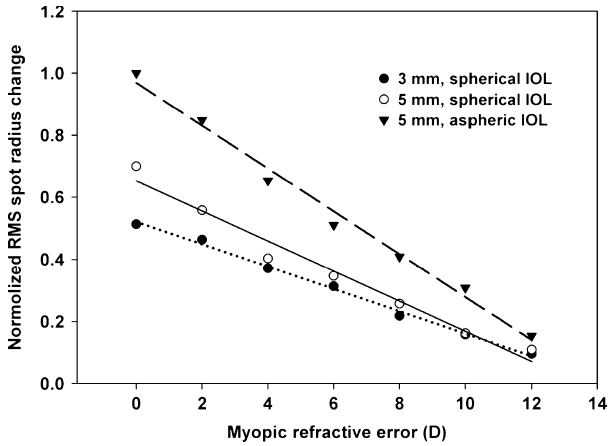

Figure 3. Normalized change of RMS spot radius due to misalignment of IOLs as a function of increased myopic refractive error. The misalignments are a combination of decentrations, tilts and axial translations. Spherical IOLs with both a 3 and a 5 mm pupil size and an aspheric IOL with a 5 mm pupil size are shown. The lines are linear regressions.

spherical IOL with 3 mm pupil size had the lowest RMS spot size change and the aspheric IOL with 5 mm pupil size had the highest. The differences between these three data sets were all significant (two tailed paired *t*-tests with 6° of freedom, $t = 5.18$ and $p = 0.002$ for the pair of spherical designs and $t = -5.18$ and $p = 0.002$ for the two pairs of spherical and aspheric designs). The lower refractive errors show the greatest differences. In *Figure 3*, aspheric IOLs that provide partial correction of spherical aberration of the eye were more sensitive to the misalignment compared to spherical ones at same refractive error level. For example, the aspheric IOL for 2D of refractive error gave 1.5 times the RMS spot radius change than the spherical IOL at the same refractive error level and pupil size. A consequence is that customized aberration correction IOLs that are designed for individual eyes are likely to be much more sensitive to position errors. This confirmed the conclusion of other studies (e.g. ref. 14). However, it is worth noting that although aspheric IOLs have the biggest spot size changes they still provided smaller spot sizes than spherical IOLs at the same pupil size. Our additional simulation results show the benefit of customized correction regardless of misalignments, since the wavefront aberrations after customized correction was still lower than for partial correction within the typical sizes of misalignment errors for customized IOLs.

Experimental results with the physical model eye

We tested two symmetrical spherical IOLs with labelled powers of 16.0D and 24.0D. *Figure 4* shows the trace of the inertia matrix and RMS radius plotted for different types of misalignment. The 24.0D IOL had a wider DPSF than the 16.0D IOL at the best focus or for any of the misalignments, which suggests that the 24.0D IOL may have had larger aberrations than the 16.0D IOL. Ray-tracing showed that the RMS of spherical aberration for the 24.0D IOL is about 50% bigger than that for the 16.0D IOL for a 3 mm pupil size. For both 24.0D and 16.0D IOLs, the curves are somewhat asymmetric, which could also be caused by non-symmetric high-order aberrations. At around the best focus, the trace value and RMS radius changes are not as rapid as the other misaligned positions. Comparing the two IOLs, we found that under most occasions the 24.0D IOL has bigger trace and RMS radius change than the 16.0D IOL when misaligned. To clarify this, *Table 1* lists the average changes across the decentration and axial translation ranges. The data unit in this table is microns (RMS) or microns square (trace) per 0.1 mm, which quantifies the change when there is 0.1 mm decentration or translation. The vertical decentration upward was not calculated due to the absence of many data points. Except for the horizontal decentration to the left (shown by the italic font in *Table 1*) measured by RMS radius, for all other misalignments, the 24.0D IOL was found to have bigger average changes than the 16.0D one, which suggests higher optical power IOLs are more sensitive to position changes.

Power distribution ratios were calculated for both 24.0D and 16.0D IOLs under all misalignments, and we calculated the ratio of the corresponding values for the two IOLs (24.0D/16.0D). We found that all ratios were smaller than one which means that the 16.0D IOL provided more concentrated light than the 24.0D IOL, regardless of any misalignment errors. This is consistent with the results shown in *Figure 4*.

Using the myopia ray-tracing eye models, we also performed ray-tracing simulations which showed that the IOL axial translation is the most sensitive of the three variables we studied. To compare the relative importance of decentrations with the axial translations by the measured data of IOLs from the model eye tests, *Figure 5* shows traces of the inertia matrix of the two IOLs as functions of horizontal decentration together with their axial translations. The equivalent effect of decentration and translations measured by the trace values can be calculated from this figure. For example, as an estimate for the 16.0D IOL, horizontal decentration to the left by 1.0 mm is equivalent to about 0.3 mm axial translation toward the retina or about 0.2 mm axial translation toward the cornea. From this figure the axial translation's important role in predicting the simulation results is confirmed. The IOL tests were performed for a 3 mm optical size. It is expected that broader DPSFs would be recorded if the functional IOL optical area were larger.

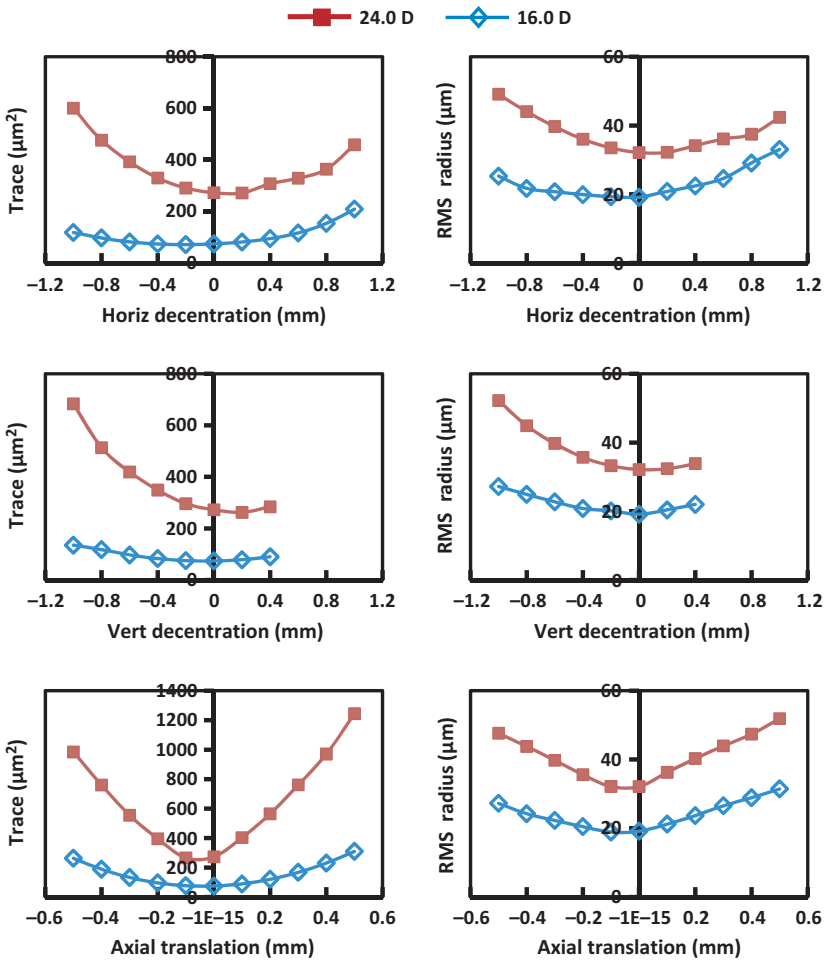

Figure 4. Trace of the inertia matrix and RMS radius changes measured in two different power IOLs with misalignments in the physical model eye. For comparison, the two IOLs are plotted together on each sub-figure. More data points of vertical decentration upward (middle sub-figures) could not be obtained due to the mechanical limitation of the design of the model eye.

Table 1. Average trace of inertia matrix change and RMS radius change measured by two different power IOLs due to five types of misalignments. The unit is micron per 0.1 mm and micron square per 0.1 mm, for RMS radius change and trace change respectively. The two italics in this table show an exceptional pair of numbers that indicate that the RMS radius change of the 24.0 D IOL did not increase more rapidly than the 16.0 D IOL, while the corresponding trace of inertia matrix does. This means that although geometrical distribution of DPSF of the 24.0 D IOL was smaller than that of the 16.0D IOL, the peak of 24.0D was more spread

		Vertical decentration downward	Horizontal decentration to left	Horizontal decentration to right	Axial translation to retina	Axial translation to cornea
16.0D	Trace of inertia change	6.10	4.41	13.48	37.80	47.04
	RMS radius change	0.81	0.61	*1.39*	1.62	2.46
24.0D	Trace of inertia change	41.07	32.79	18.62	142.32	194.30
	RMS Radius change	2.01	1.69	*1.02*	3.10	3.95

Discussion and conclusion

Root mean square radius and trace of inertia matrix both gave the information about the size of the DPSF. The RMS radius was calculated from all signal pixels without weighting signal intensity (*Equation 1*), which gave an estimate of the geometrical distribution. The trace of inertia matrix was pixel signal intensity (*Equation 2*)

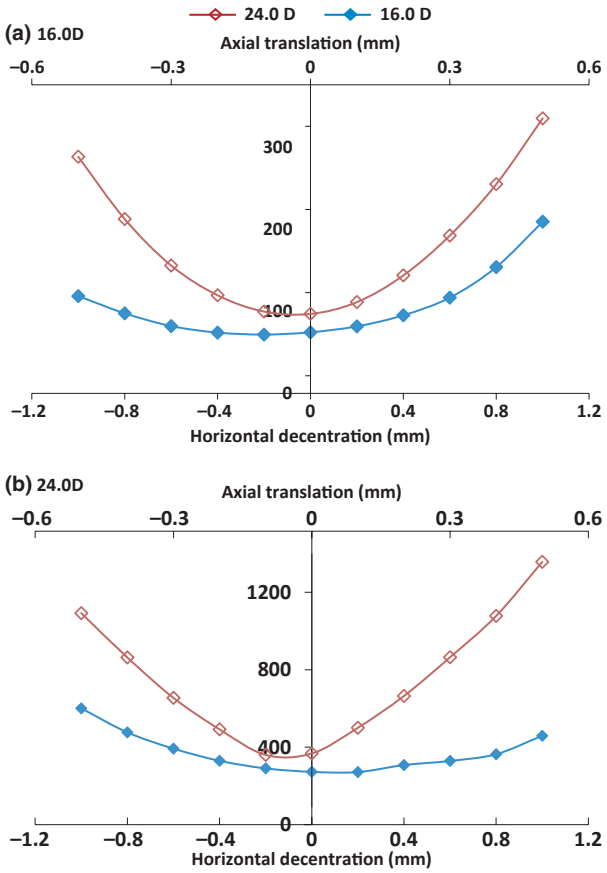

Figure 5. 16.0D and 24.0D IOLs' trace of inertia matrix change with horizontal decentration and axial translations. In both (a) and (b), the top horizontal axis scale is for axial translation in millimetres and the bottom horizontal axis scale is for horizontal decentration in millimetres. The vertical axes are the trace in microns square.

weighted and it measured how intensity spread the peak value of the DPSF to its neighbourhood.[28] Regarding the misalignment effects of two different power IOLs (see *Table 1*), for the horizontal decentration to the left the DPFS of the 24.0 D IOL did not increase more rapidly than 16.0 D as measured by the RMS radius, while it did when measured by the trace of inertia matrix. This means that although the geometrical distribution of DPSF of the 24.0 D IOL is smaller than that of the 16.0D IOL, the peak of the 24.0D IOL is more spread.

The DPSF does not provide spatial frequency information about the IOLs, as provided by MTF measurements. Considering our purpose was to compare the effect of misalignment of different powered IOLs, the measurement and data processing in the current study were simple and provided useful results. The PSF measurement not only includes aberrations but also reflects the light scatter by the IOL. Some previous studies measured the IOL single path PSFs.[29,30] It is not possible to directly compare our results with those due to different optical magnification, pupil sizes, and optical powers. Our power ratio results shows that a higher power IOL had relatively less power distribution around the centroid of the DPSF compared to a lower power IOL, which confirms a similar finding by Rawer *et al.*[31]

As a general conclusion, spherical or aspheric IOLs designed for patients with larger amounts of myopia are less sensitive to IOL implantation position errors, compared to the IOLs designed for patients with less myopia. Obviously, more myopic eyes need lower powered IOLs and have an increased optical tolerance to position errors of the IOL. Under the same conditions, aspheric IOLs are more sensitive to misalignments than spherical IOLs. Hyperopic eyes have not been included in this study but we may extrapolate the curves from the main ray-tracing results (*Figure 3*) to the hyperopic side. We expect that a steeper change would occur which would predict that IOLs for hyperopic eyes would be even more sensitive to their implantation positions. This would help to explain why hyperopic patients have more complains about their vision after cataract surgery.

Acknowledgements

We thank Elie DeLestrange for his assistance with the experiments. We are grateful for financial support from the Enterprise Ireland International Research Fund (IR-2008-0014) and Science Foundation Ireland (07/IN.1/1906).

References

1. Atchison DA. Optical design of intraocular lenses. I. On-axis performance. *Optom Vis Sci* 1989; 66: 492–506.
2. Atchison DA. Design of aspheric intraocular lenses. *Ophthalmic Physiol Opt* 1991; 11: 137–146.
3. Holladay JT, Piers PA, Koranyi G, van der Mooren M & Norrby NE. A new intraocular lens design to reduce spherical aberration of pseudophakic eyes. *J Refract Surg* 2002; 18: 683–691.
4. Tabernero J, Piers PA & Artal P. Intraocular lens to correct corneal coma. *Opt. Letters* 2007; 32: 406–408.
5. Artal P, Manzanera S, Piers P & Weeber H. Visual effect of the combined correction of spherical and longitudinal chromatic aberrations. *Opt Express* 2010; 18: 1637–1648.
6. Kempen JH, Mitchell P, Lee KE *et al.* The prevalence of refractive errors among adults in the United States, Western Europe, and Australia. *Arch Ophthalmol* 2004; 122: 495–505.
7. Yekta AA, Fotouhi A, Khabazkhoob M *et al.* The prevalence of refractive errors and its determinants in the elderly population of Mashhad, Iran. *Ophthalmic Epidemiol* 2009; 16: 198–203.

8. Sawada A, Tomidokoro A, Araie M, Iwase A & Yamamoto T. Refractive errors in an elderly Japanese population: the Tajimi study. *Ophthalmology* 2008; 115: 363–370 e3.
9. Atchison DA. Optical models for human myopic eyes. *Vision Res* 2006; 46: 2236–2250.
10. Foster PJ, Broadway DC, Hayat S *et al.* Refractive error, axial length and anterior chamber depth of the eye in British adults: the EPIC-Norfolk Eye Study. *Br J Ophthalmol* 2010; 94: 827–830.
11. Wickremasinghe S, Foster PJ, Uranchimeg D *et al.* Ocular biometry and refraction in Mongolian adults. *Invest Ophthalmol Vis Sci* 2004; 45: 776–783.
12. Shammas H, editor. *Intraocular Lens Power Calculation*. SLACK Incoporated: New Jersey, 2004.
13. Norrby S, Piers P, Campbell C & van der Mooren MD. Model eyes for evaluation of intraocular lenses. *Appl Opt* 2007; 46: 6597–6605.
14. Piers PA, Weeber HA, Artal P & Norrby S. Theoretical comparison of aberration-correcting customized and aspheric intraocular lenses. *J Refract Surg* 2007; 23: 374–384.
15. Guo HQ, Wang ZQ, Zhao QL, Quan W & Wang Y. Individual eye model based on wavefront aberration. *Optik* 2005; 116: 80–85.
16. Altmann GE, Nichamin LD, Lane SS & Pepose JS. Optical performance of 3 intraocular lens designs in the presence of decentration. *J Cataract Refract Surg* 2005; 31: 574–585.
17. Hong X & Zhang X. Optimizing distance image quality of an aspheric multifocal intraocular lens using a comprehensive statistical design approach. *Opt Express* 2008; 16: 20920–20934.
18. Zhao H. Optical ensemble analysis of intraocular lens performance through a simulated clinical trial with ZEMAX. *Opt Lett* 2009; 34: 7–9.
19. Akkin C, Ozler SA & Mentes J. Tilt and decentration of bag-fixated intraocular lenses – a comparative-study between Capsulorhexis and Envelope Techniques. *Doc Ophthalmol* 1994; 87: 199–209.
20. Auran JD, Koester CJ & Donn A. In vivo measurement of posterior chamber intraocular lens decentration and tilt. *Arch Ophthalmol* 1990; 108: 75–79.
21. de Castro A, Rosales P & Marcos S. Tilt and decentration of intraocular lenses in vivo from Purkinje and Scheimpflug imaging - Validation study. *J Cataract Refract Surg* 2007; 33: 418–429.
22. Mutlu FM, Bilge AH, Altinsoy HI & Yumusak E. The role of capsulotomy and intraocular lens type on tilt and decentration of polymethylmethacrylate and foldable acrylic lenses. *Ophthalmologica* 1998; 212: 359–363.
23. Petternel V, Menapace R, Findl O *et al.* Effect of optic edge design and haptic angulation on postoperative intraocular lens position change. *J Cataract Refract Surg* 2004; 30: 52–57.
24. Phillips P, Perez-Emmanuelli J, Rosskothen HD & Koester CJ. Measurement of intraocular lens decentration and tilt in vivo. *J Cataract Refract Surg* 1988; 14: 129–135.
25. Lu B & Shen Z. [Measurement and research of posterior chamber intraocular lens tilt and decentration in vivo]. *Zhonghua Yan Ke Za Zhi* 1999; 35: 40–42.
26. International Organization for Standardization. 11979-2, Ophthalmic implants - intraocular lenses – Part 2: optical properties and test methods. 1999.
27. International Organization for Standardization. 24157, Ophthalmic optics and instruments – Reporting aberrations of the human eye. 2008.
28. Caprari RS. Method of target detection in images by moment analysis of correlation peaks. *Appl Opt* 1999; 38: 1317–1324.
29. Mitchell L, Molteno AC, Bevin TH & Sanderson G. Star testing: a novel evaluation of intraocular lens optical quality. *Br J Ophthalmol* 2006; 90: 586–592.
30. Pieh S, Marvan P, Lackner B *et al.* Quantitative performance of bifocal and multifocal intraocular lenses in a model eye: point spread function in multifocal intraocular lenses. *Arch Ophthalmol* 2002; 120: 23–28.
31. Rawer R, Stork W, Spraul CW & Lingenfelder C. Imaging quality of intraocular lenses. *J Cataract Refract Surg* 2005; 31: 1618–1631.